

Parameter Identification Procedure for Hysteretic Shear-Resistant Properties of Beech Wood Dowels

Jiwei Liu,^{a,*} Huifeng Yang,^{b,*} Yutao Zhou,^b Benkai, Shi,^b and Haotian Tao^a

To evaluate the shear-resistant behavior of wooden dowels used in Blockhaus shear walls under cyclic load, 19 specimens under ten groups of conditions were prepared and tested. The failure modes, hysteresis curves, mechanical properties, stiffness degradations, and energy dissipation capacities of the specimens were studied. The test results showed that with the increase in the number of dowels, the initial stiffness and peak load of the specimens increased greatly. The diameter of the dowels had little influence on the mechanical properties of the specimens. Furthermore, the test findings demonstrated that the pretension load between the walls greatly enhanced the initial stiffness and energy dissipation capacity of specimens. A simplified finite element model was established in Opensees. Considering the effect of material variability, the parameters of single dowel shear spring and friction spring were identified by Genetic Algorithm with modified objective function in Matlab. The identified parameters were applied to the finite element model of the multi-dowel specimens. The simulation results were in good agreement with the test results, and the validity of the numerical model and parameter identification method was verified.

DOI: 10.15376/biores.19.2.3681-3698

Keywords: Wooden dowels; Blockhaus shear walls; Hysteretic behavior; Parameter identification

Contact information: a: School of Civil Engineering, Southeast University, Nanjing, 211189, China;

b: College of Civil Engineering, Nanjing Tech University, Nanjing, 211816, China;

* Corresponding authors: 945290530@qq.com; hfyang@njtech.edu.cn

INTRODUCTION

This paper considered the shear performance of wooden dowels in *Blockhaus* shear walls under cyclic load. *Blockhaus* structure is a timber structure made by overlapping square timbers, as shown in Fig. 1. It has been shown that *Blockhaus* shear walls exhibit greater lateral resistance than light wood shear walls and similar hysteretic properties to concrete shear walls (Graham *et al.* 2010; Branco and Araújo 2012). Additionally, *Blockhaus* timber structures show great seismic performance during both the experiments and actual usage (Branco *et al.* 2013; Tomasi and Piazza 2013). Therefore, *Blockhaus* structures are widely built in areas of the world having a high percentage of forest cover (Bedon and Fragiaco 2019; Sciomenta *et al.* 2020).

Square timber shear walls show an obvious load resistance mechanism. The vertical load-resistant ability of traditional *Blockhaus* wall is determined by the compression strength of timber perpendicular to the grain and by the contact area. The ability to resist horizontal load is mostly dependent on the friction between the timber pieces, the interlock between orthogonal walls, and dowel-type members between the timbers (Hirai *et al.* 2004).

Although the *Blockhaus* building has been shown to have satisfactory seismic performance, the non-structural damage brought on by sliding between logs is still

substantial. Thus, in a *Blockhaus* structure, a sensible and secure anti-lateral load mechanism must be implemented. The following conclusions have been drawn through the research: (i) The lateral load-resistant ability of *Blockhaus* shear walls can be calculated by the superposition of each lateral load-resistant element; (ii) The primary energy dissipation capability of the structure is provided by friction between interfaces; and (iii) If the wooden dowels are properly designed, the lateral load resistance ability offered by the dowels will be substantially greater than that offered by the interlock between orthogonal log walls (Hirai *et al.* 2004; Scott *et al.* 2005a,b). The horizontal resistance of the *Blockhaus* shear wall is significantly influenced by the friction between the timber pieces and the dowel-type shear components. The combination of friction and dowel-type shear components effectively reduces the relative displacement between the timbers and the non-structural damage caused by sliding between them if the dowel-type components are designed and built properly. However, under normal design conditions or under specific pressures such as earthquakes, the currently existing European standards do not include an analytical model for the shear resistance of wooden dowels in the *Blockhaus* shear wall (EN 1995-1-1 2004; EN 1998-1 2004). Nevertheless, the vast majority of studies on the shear contribution element ignore the impact of friction and wooden dowels in favor of concentrating on interlock between orthogonal log walls of the shear walls. As shown in Fig. 1, orthogonal timber walls involve cross-bite connections among the timbers for adjoining walls (Branco and Araújo 2010; Giovannini *et al.* 2014; Grossi *et al.* 2016; Sciomenta *et al.* 2018). Therefore, it is difficult to accurately predict and evaluate the load bearing capacity and seismic performance of the *Blockhaus* structure, which limits its design and application.

As for the numerical model, it turns out that it is challenging to precisely model the solid finite element simulation of dowel-type components in timber structures concerning the use of dowel-type components in other timber systems. The primary reason is that macroscopic timber property tests are typically used to determine the timber mechanical properties used in the finite element model. In contrast, the early stage of timber damage between the dowel-type components and timber material in the push-out test is miniscule. As a result, the shear components of dowel-type connectors frequently have an excessively high initial stiffness estimate using solid finite element simulation (Wang *et al.* 2018). Furthermore, the mechanical properties of wooden dowels are influenced by the properties of timber materials and the randomness of defects. Therefore, there are some differences in the shear performance of wooden dowels with the same geometric parameters (Lam *et al.* 2008; Wang *et al.* 2016, 2019).

Considering the limitations of previous research, in this paper the influence of the number and diameter of the wooden dowels and vertical pretension load on the shear mechanical properties of the dowels was analyzed. Considering the limitation of the initial stiffness analysis of the solid element numerical model of the shear components in timber structures, a simplified numerical model was established in the Opensees environment. Multiple groups of test data under the same experimental conditions were applied to the parameter identification program (Genetic Algorithm), considering the randomness of timber properties and defects. To determine the parameters for the single dowel and friction spring, the modified objective function is the square sum of the differences between each group of test data and the model data. The identified parameters were then applied to the multi-dowel specimens to compare the test results with the results of the numerical model. The validity of the numerical model and the parameter identification method were confirmed.

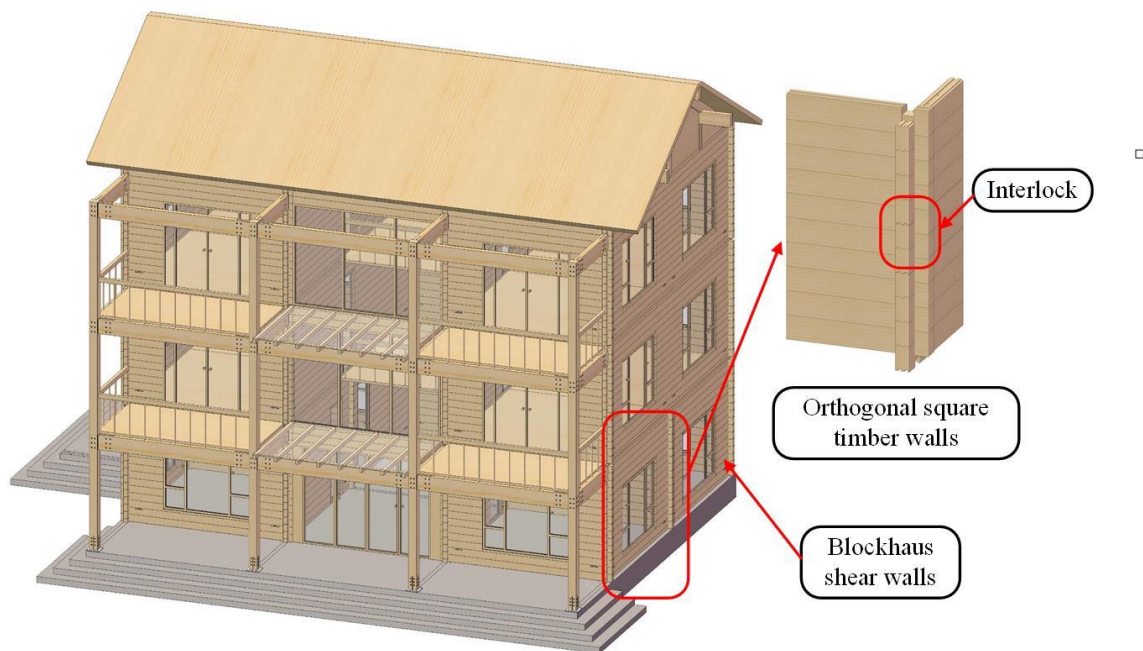


Fig. 1. Blockhaus shear walls and orthogonal log walls

EXPERIMENTAL TEST

Test Specimens

The goal was to evaluate and compare the effects of wooden dowel diameter, number, and pretension load on shear-resistant performance. The primary design information of the specimens is shown in Table 1. *Pinus sylvestris* glulam (glued laminated timber) was used to manufacture rectangular timber pieces. The dimensions of timber pieces used in test structures were 105(T) mm \times 850(L) mm \times 180(R) mm. The dowels were made of beech. The length of each dowel was 540 mm, and the diameter was selected according to different working conditions, as shown in Table 1. The primary properties of timber material were obtained by material testing according to European code (EN 408:2010+A1 2012), as shown in Table 2.

Table 1. Test Information of Hysteretic Shear Test of Wooden Dowels

Test ID	Number of Specimens	Pretension Load (kN)	Diameter (mm)	Number of Dowels	Space (mm)
P10	3	10	-	0	-
P0D25	2	0	25	1	-
P0D35	2	0	35	1	-
P0D30	3	0	30	1	-
P10D30	1	10	30	1	-
P0D30-300-2	2	0	30	2	300
P10D30-600-2	1	10	30	2	600
P0D30-600-2	2	0	30	2	600
P10D30-300-3	1	10	30	3	300
P0D30-300-3	2	0	30	3	300

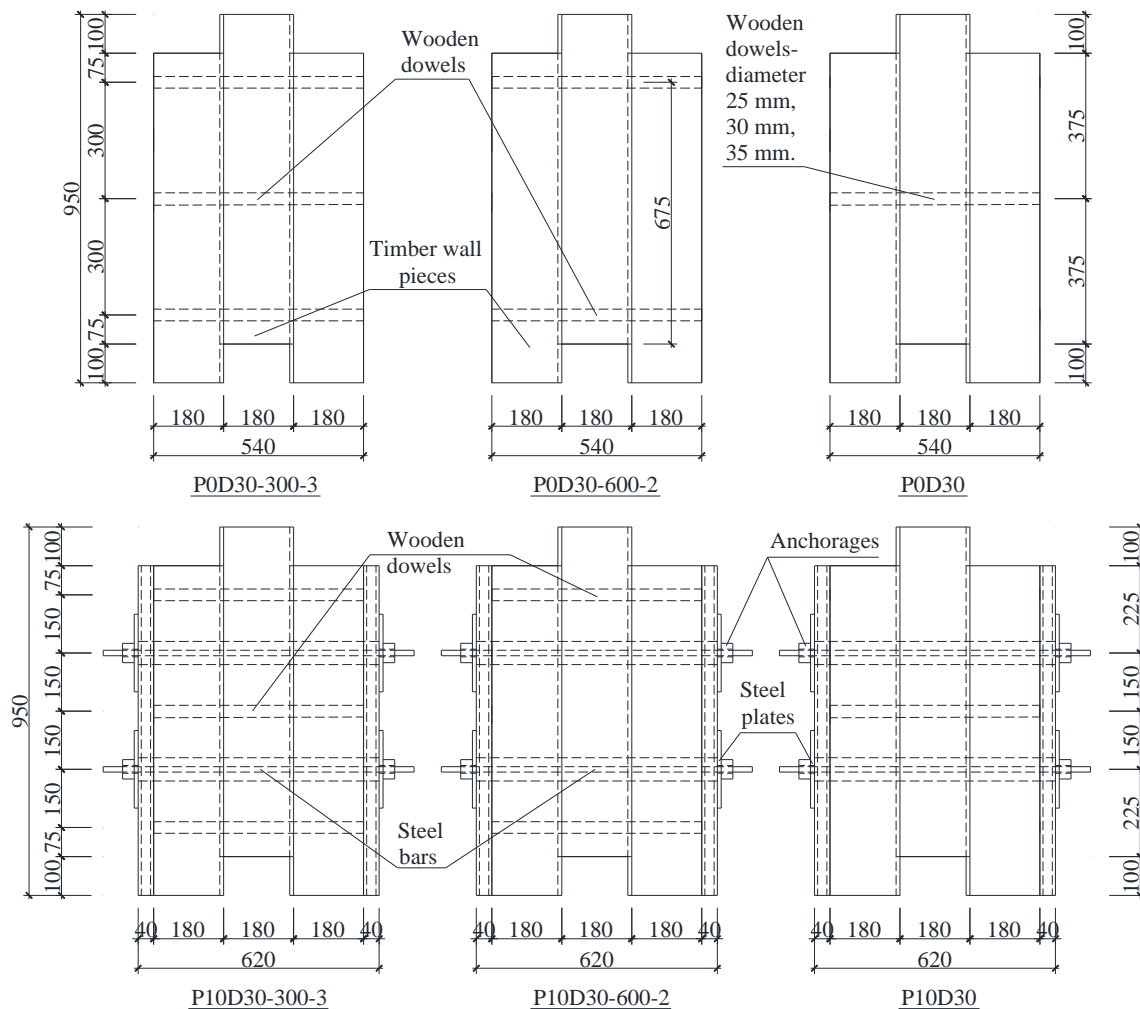
Table 2. Physical and Mechanical Properties of Timber Material

Material	Density (g/cm ³)	Moisture Content (%)	Compressive Strength Parallel to Grain (MPa)	Young's Modulus (MPa)
<i>Pinus sylvestris</i>	0.446	13.24	33.2	10247
Beech	0.668	12.67	-	15913

Grade 235 steel with a yield strength of 235 MPa and elastic modulus of 200 GPa was used to manufacture the steel brackets and plates. The yield strength of the steel bars used to apply the pretension load was 640 MPa and the diameter of steel rods was 14 mm. The detailed geometries and specimen sizes are shown in Fig. 2.

Test Setup and Loading Procedure

The loading device and measurement instruments of the specimens are shown in Fig. 4, including (a) Test setup; (b) Loading procedure; and (c) Preliminary test.

**Fig. 2.** Geometry of test specimens

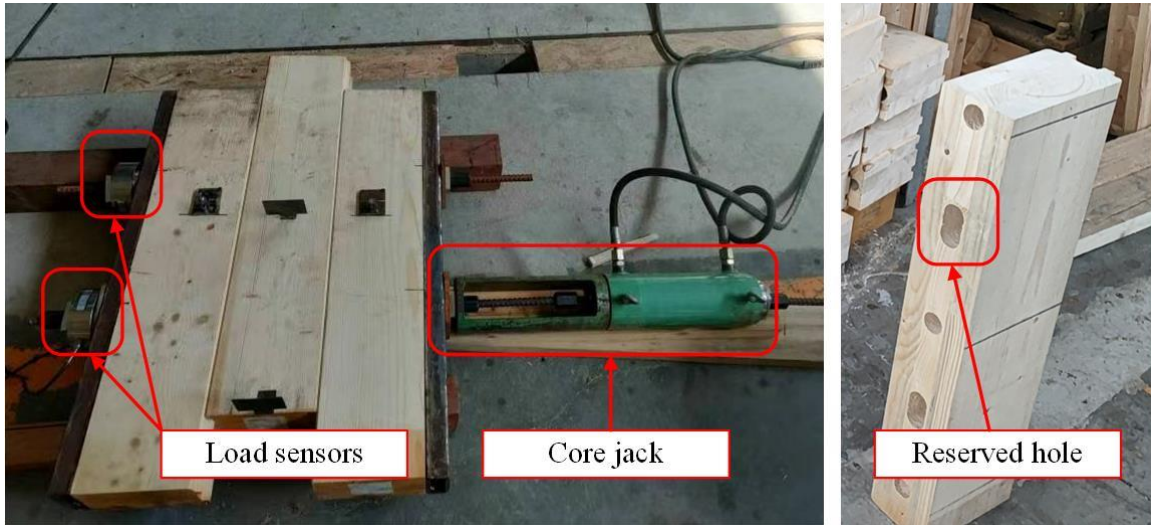


Fig. 3. Pretension load application diagram and timber logs

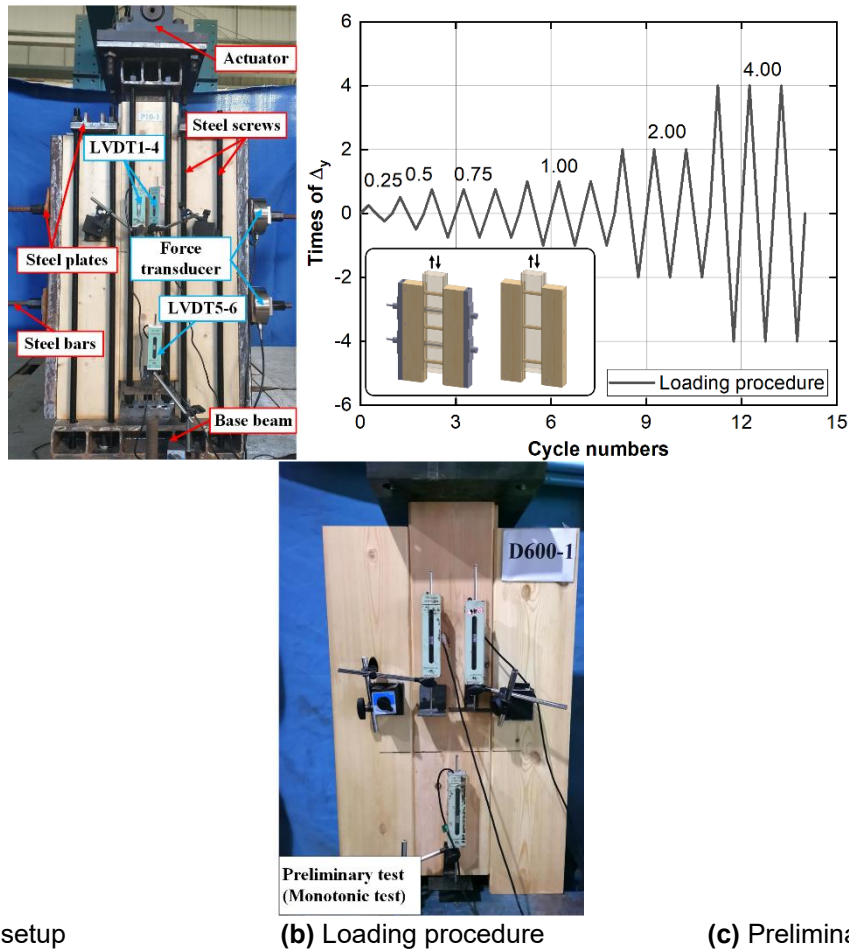


Fig. 4. Test set-up and loading procedure

Figure 4(a) shows the two sides of the walls fastened to the reaction frame by the steel plates and screws. Linear variable displacement transformers (LVDTs) 1 to 4 were used to measure the relative displacement between walls. The LVDTs 5 and 6 arranged at

the bottom of the middle walls recorded the absolute displacements of the specimens. Two force sensors recorded the changes in pretension load in steel rods.

The specimen designed with pretension load was preloaded through the core jack and the screw-thread steel bars, as shown in Fig. 3(a). When the nut was screwed well on one side, the special steel member and the core jack were used to stretch the steel bars on the other side. Finally, the nut at the tension section was tightened to realize the pretension force. The pressure sensor was used to test whether the pretension force reached the design value, and the hysteresis cycle test was carried out immediately after the end of the tension. In order to prevent the screw from being sheared during the loading process, the reserved hole for the screw in timber logs was enlarged (an oval hole with a length of 60 mm) according to the ultimate displacement obtained from the monotonic test results, as shown in Fig. 3(b). The steel plate was positioned to control the central position of the screw in the reserved hole, to ensure that the screw did not shear during the loading process.

A 300 kN actuator was fastened to the middle wall using steel plates and screws to apply cyclic loads. The loading protocol refers to the loading method in European code (EN 12512 2001), as illustrated in Fig. 4(b), where the loading displacement uses a multiple of the yield displacement. The peak displacement of the first two cycles was 0.25 and 0.5 times the yield displacement, respectively. The remaining loading steps used 0.75, 1, 2, and 4 times the yield displacement, respectively. Each step was performed for three cycles. The yield displacements of the specimens were selected according to the preliminary monotonic tests, as shown in Fig. 4(c) (Wang 2018).

SIMULATION METHODS

Failure Modes

The failure mode of the specimen is shown in Fig. 5. Local crushing damage can be found around the reserved holes in the timber walls due to the compression of wooden dowels. Shear failure of the dowels due to cyclic load can be observed in Fig. 5(a).

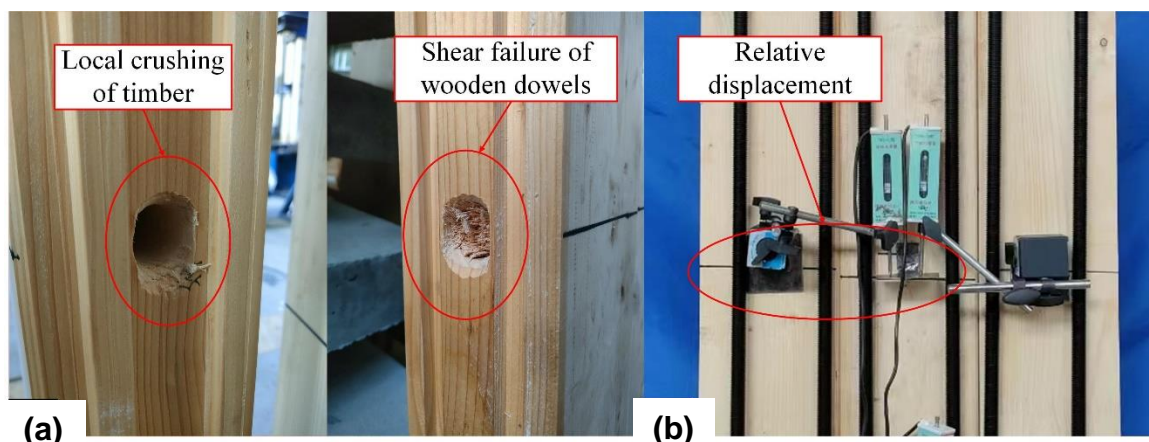
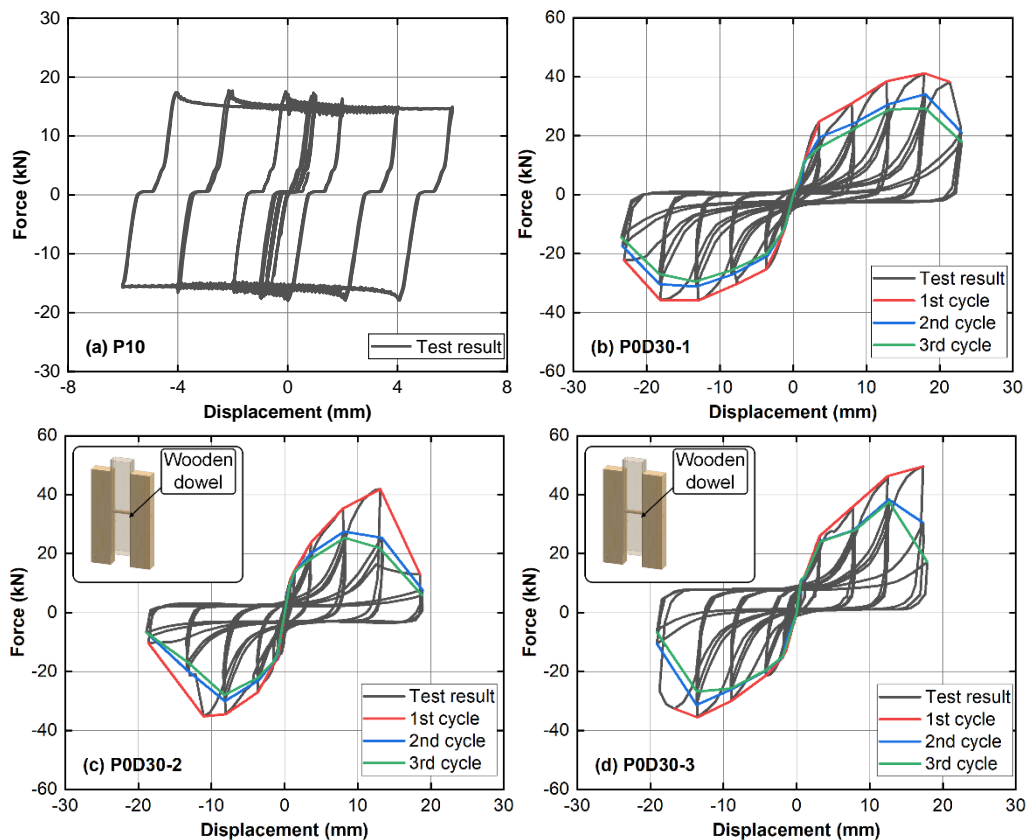


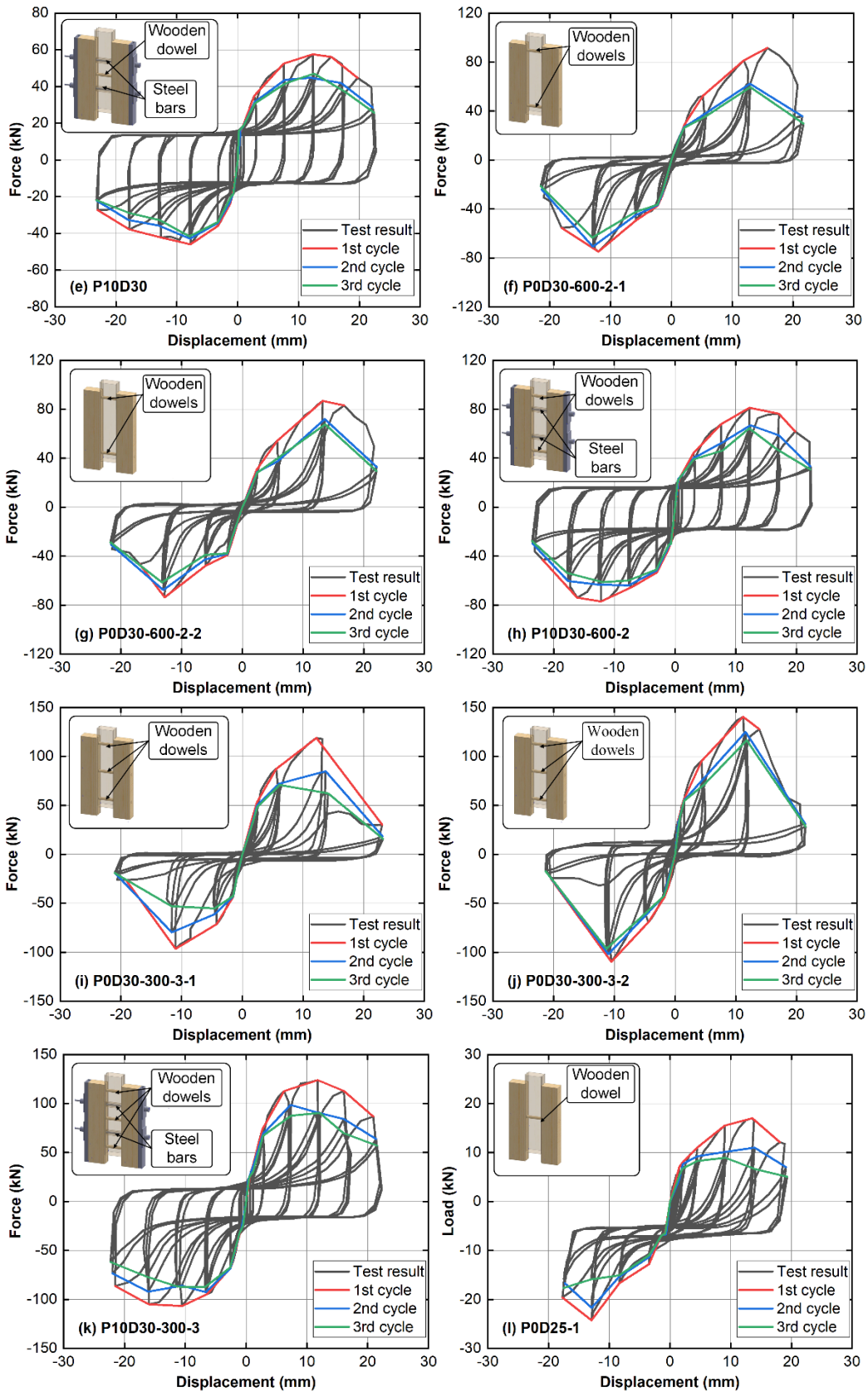
Fig. 5. Failure modes of specimens

Hysteresis Curves and Mechanical Properties

The hysteretic curves of load-relative displacement of the specimen recorded from the cyclic tests are shown in Fig. 6. Hysteretic behavior of the specimen with pretension load and without dowels is illustrated in Fig. 6(a). The response force of this specimen is

generated only by the friction of the contact surface. The hysteresis curve of one group is shown in Fig. 6(a), because the results of the three groups were similar. The specimen's hysteretic curve was full and almost identical to the specimen with ideal elastoplastic behavior. Before the sliding of the test specimens, static friction provided anti-shear force, as shown in the elastic stage in Fig. 6(a). After the sliding of the test specimens, dynamic friction provided shear force, as shown in the yield stage in Fig. 6(a). The relative displacement can be observed in Fig. 5(b). Considering the short-term test, the creep behavior of timber under long-term compression was not considered in this paper. The following conclusions can be drawn from the hysteresis curves in Figs. 6(b) to 6(n): (i) Specimens with pretension load had the fuller shape of hysteretic curves; (ii) With the increase of the number of dowels, the peak load of the specimens increased greatly; (iii) The peak load of each specimen with a single dowel without pretension load was similar. However, the load-decreasing section and the ultimate displacement were quite different among the above-mentioned specimens due to the randomness of properties and defects of timber material.





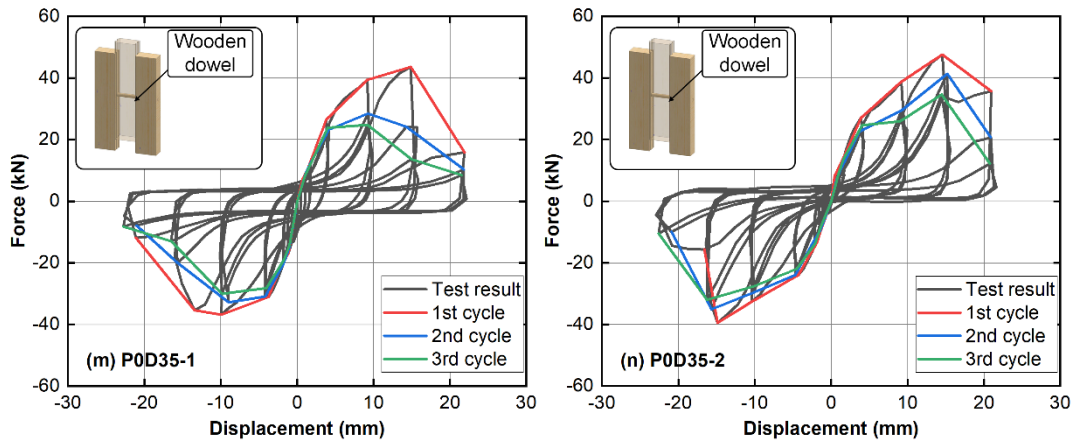


Fig. 6. Force-displacement hysteresis curves (test values)

The mechanical properties are summarized and illustrated in Table 3. These mechanical properties were calculated according to the calculation method provided in European code (EN 12512 2001). According to the calculation results of mechanical properties, the following conclusions can be drawn: (i) With the increase of the number of wooden dowels, the initial stiffness, yield load, and peak load of the specimen were increased significantly; Compared with the single-dowel specimens, the initial stiffness and peak load of the double-dowel specimen were increased 100.4% and 108.0%, respectively, and those of the three-dowel specimen were increased 278.0% and 196.2%, respectively. (ii) The pretension load had a great impact on the initial stiffness of the test specimen, a great impact on the ultimate load-bearing capacity of specimens with single dowel, and a little impact on the ultimate load-bearing capacity of specimens with multi-dowels; For single dowel and double dowel specimens, the initial stiffness of specimens with initial pretension load increased 165.2% and 89.8%, respectively. (iii) The initial stiffness, yield load, and ultimate load-bearing capacity of the specimens increased with the increase of the diameter of the wooden dowel.

Table 3. The Main Results of the Reversed Cycle Loading Test

Test ID		K_i	Δ_y	F_y	Δ_{max}	F_{max}	Δ_u
P0D30	Positive	7.27	3.43	24.83	16.1	44.19	19.08
	Negative	7.44	3.09	22.61	11.52	34.34	17.58
	Mean	7.36	3.26	23.72	13.81	39.27	18.33
P10D30	Positive	15.12	2.68	40.51	12.35	57.52	19.72
	Negative	23.92	1.07	25.59	7.75	45.94	23.03
	Mean	19.52	1.88	33.05	10.06	51.73	21.37
P0D600-2	Positive	11.39	4.54	51.69	14.51	89.10	16.28
	Negative	18.11	2.08	37.36	12.39	74.27	17.47
	Mean	14.75	3.31	44.53	13.45	81.69	16.87
P10D600-2	Positive	17.55	3.18	55.80	12.28	81.21	19.79
	Negative	38.45	1.07	41.14	12.19	77.12	21.83
	Mean	28.00	2.13	48.47	12.23	79.17	20.81
P0D300-3	Positive	28.89	2.97	81.61	11.70	129.49	18.46
	Negative	26.76	2.28	60.77	10.75	103.14	19.84
	Mean	27.82	2.62	71.19	11.22	116.31	19.15
P10D300-3	Positive	28.54	3.52	100.44	11.79	123.79	20.91
	Negative	28.43	2.77	78.74	10.53	106.67	21.52

	Mean	28.48	3.15	89.59	11.16	115.24	21.22
P0D25	Positive	4.85	1.46	7.08	13.56	17.01	18.10
	Negative	3.55	3.32	11.77	12.93	24.25	17.73
	Mean	4.20	2.39	9.425	13.24	20.63	17.91
P0D35	Positive	6.94	4.97	34.45	14.70	45.57	21.44
	Negative	10.99	2.68	25.09	14.15	38.16	18.86
	Mean	8.96	3.83	29.77	14.42	41.87	20.15

Notes: In the table, K_i is the initial stiffness. Δ_y is the yield displacement. F_y is the yield force. Δ_{max} is the corresponding displacement to the maximum load. F_{max} is the maximum load. Δ_u is the ultimate displacement.

Degradation of Stiffness and Dissipation of Energy

To compare the stiffness degradation of specimens subjected to cyclic loads under various loading stages. The secant stiffness of specimens was calculated by Eq. 1 in accordance with the equation provided by the Chinese code (JGJ/T 101 2015),

$$K_i = \frac{|F_{i+}| + |F_{i-}|}{|\Delta_{i+}| + |\Delta_{i-}|} \tag{1}$$

where K_i is the secant stiffness of specimens at i th loading step. F_{i+} and F_{i-} are the force of specimens at the i th loading step in positive and negative directions, respectively. Δ_{i+} and Δ_{i-} are the displacement at the i th loading step in positive and negative direction, respectively.

According to the European standard (EN 12512 2001), the energy dissipation capacity of dowels was calculated using Eq. 2,

$$v_{eq} = \frac{1}{2\pi} \cdot \frac{E_d}{E_p} \tag{2}$$

where v_{eq} is the equivalent viscous damping coefficient of specimens; E_d is the energy dissipation per cycle; and E_p is the ideal potential energy dissipation per cycle.

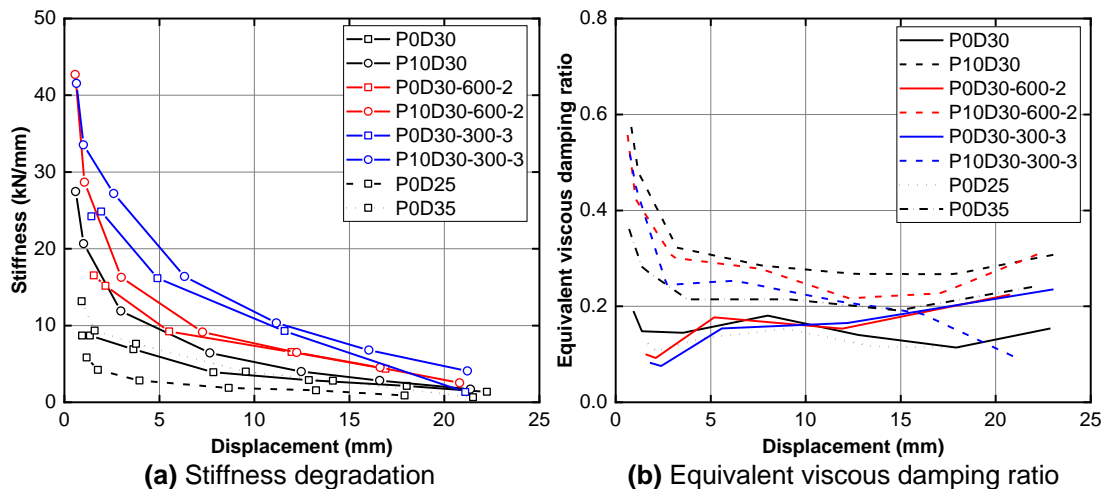


Fig. 7. Equivalent viscous damping ratio and stiffness degradation (test values)

The calculation results of stiffness degradation and equivalent viscous damping ratio are shown in Fig. 7: (a) Stiffness degradation; (b) Equivalent viscous damping ratio. It is evident that the pretension load and the number of dowels significantly affected the initial stiffness of specimens. The application of pretension load was able to successfully increase the initial stiffness of specimens, but as loading displacement increased, the influence of pretension load on the stiffness of specimens decreased. With the increase in the number of wooden dowels, the stiffness increased greatly throughout the whole loading process. It can be seen from Fig. 7(b) that the energy dissipation capacity of specimens greatly increased due to the application of pretension load, particularly when the loading displacement was smaller than 5 mm. However, the quantity and diameter of dowels had little influence on the energy dissipation capacity of the specimens.

PARAMETER IDENTIFICATION PROCEDURE AND NUMERICAL ANALYSIS

Parameter Identification Procedure and Numerical Model

The initial stiffness of specimens simulated by the solid element model of shear components established by Abaqus is typically too great because of the local microscopic degradation of wood, as illustrated in Fig. 5(a) (Wang *et al.* 2018). Therefore, in this paper, a simplified model of dowels specimens was built in Opensees environment, as shown in Fig. 8. The shear mechanical behavior of dowels and friction were simulated by uniaxial shear spring (red spring, and blue spring, respectively), as illustrated in Fig. 8. Pinching4 material provided in Opensees was chosen for simulation of the wooden dowel based on the shape of the dowels' relative displacement-load hysteresis curves. Sixteen parameters were used to simulate the skeleton curve shape of the hysteresis curve, six parameters were used to model the unloading path, and fifteen parameters were used to model the strength and stiffness degradation in Pinching4 material. Therefore, a more precise model of the shear mechanical behavior of the wooden dowel could be achieved as long as the parameters were chosen properly. The ElasticPP material, an ideal elastoplastic model, was used to model the frictional mechanical behavior between timber pieces. The parameters of the friction model (friction coefficient correlation) were identified by using the Genetic Algorithm and hysteresis curve parameters of the specimens with only pretension load and no dowels. The dispBeamColumn element provided in Opensees was used to simulate the timber logs and fiber unit is used to simulate the cross-section. Considering that the tensile and compressive constitutive behavior of timber parallel to the grain is similar to that of concrete, Concrete02 material provided in Opensees was used to simulate timber material of logs as recommended by Li *et al.* (2018), because only the tensile and compressive behavior of timber parallel to the grain were considered in the model. The material parameters of timber were selected according to the results of the timber property test, as shown in Table 2.

According to the above-mentioned content, an accurate simulation of the shear mechanical behavior of dowels can be achieved by appropriate parameters. Consequently, the following is the procedure used in this paper to identify parameters. First, the characteristics of the shear mechanical behavior produced by a single dowel and pretension load were identified, respectively, as shown in Fig. 8. Secondly, the single dowel finite element model was fitted using the identified parameters, and the accuracy was verified by comparing it with the test results. Ultimately, the identified parameters were applied to the multi-dowels model.

The parameter identification procedure in this work was carried out in Matlab and Openses environments, and Genetic Algorithm was used to identify the parameters of the Pinching4 model, as illustrated in Fig. 8. The hysteretic curves shown in Figs. 6(b) to 6(d) illustrates that specimens with single dowel construction had similar initial stiffness and peak load but differed greatly in the failure stage. The potential explanation is that timber properties and defects are random. Therefore, it is difficult to select the hysteresis curve of the specimen for parameter identification. To fully obtain the information from multiple specimens with same working condition and obtain more persuasive parameter results, the square sum of the difference between the three specimens with single dowel of test values and the simulation results of the objective function was selected here, as shown in Eqs. 3 to 5.

$$E_i = (F_{TRI,1} \quad F_{TRI,2} \quad \dots \quad F_{TRI,j}) \quad (3)$$

$$N_i = (F_{NMI,1} \quad F_{NMI,2} \quad \dots \quad F_{NMI,j}) \quad (4)$$

$$f = \sum_{i=1}^n (E_i - N_i) \cdot (E_i - N_i)^T \quad (5)$$

where E_i and N_i are the experimental and numerical load matrix of i^{th} specimen, respectively; $F_{TRI,j}$ and $F_{NMI,j}$ are the experimental and numerical load of i^{th} specimen at j^{th} load step, respectively; and f is the objective function used in Genetic Algorithm.

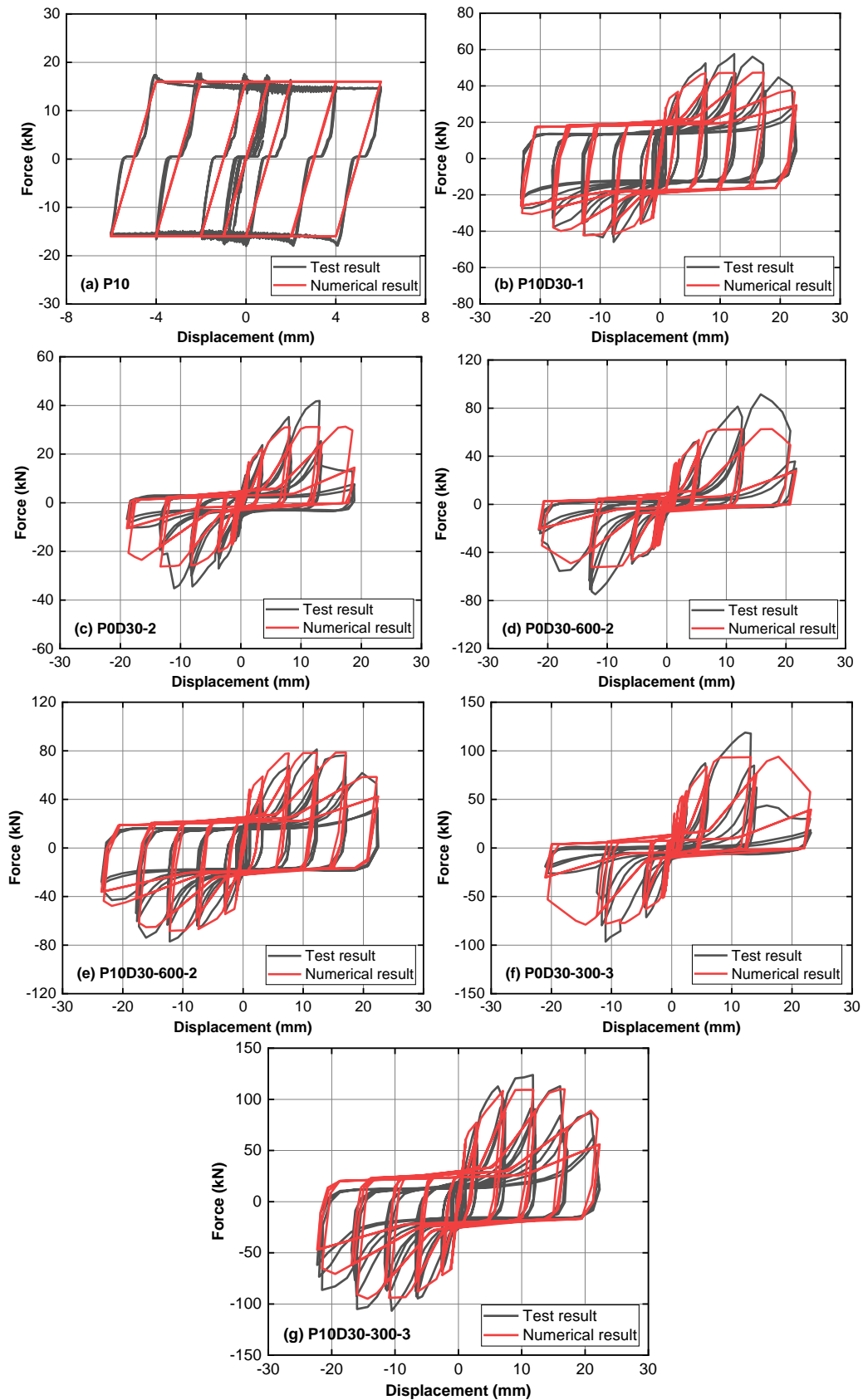


Fig. 9. Hysteresis curve comparison (test values and numerical values)

For specimens with a single dowel, the numerical result was accurate at the initial loading stage, but the difference between peak load and load decreasing stage between simulation and test was large. However, the potential reason is that the numerical result was obtained by considering all the specimens with a single dowel. Then, the identified parameters were applied to the numerical model with a single dowel and pretension load and the numerical model with multiple dowels. The hysteretic curves are shown in Figs. 9(c) to (g). It is evident that for the specimens without pretension load, the simulation performed well during the initial loading stage but poorly throughout the load-dropping stage. The whole hysteretic curves of the specimens with pretension load were accurately simulated by comparing the hysteretic curve between the numerical model and the test result. The accuracy of the parameters and the validity of the parameter identification method was confirmed.

Table 4. Identified Parameters (Numerical model)

Pinching4 Material Parameters							
F_{P1}	10.37 kN	F_{P2}	20.84 kN	F_{P3}	21.08 kN	F_{P4}	11.84 kN
F_{N1}	-11.05 kN	F_{N2}	-17.32 kN	F_{N3}	-17.77 kN	F_{N4}	-8.78 kN
Δ_{P1}	0.78 mm	Δ_{P2}	7.04 mm	Δ_{P3}	17.87 mm	Δ_{P4}	23.67 mm
Δ_{N1}	-0.88 mm	Δ_{N2}	-7.57 mm	Δ_{N3}	-14.90 mm	Δ_{N4}	-23.62 mm
r_{DP}	3.78e-1	r_{DN}	3.05e-1	r_{FP}	1.88e-1	r_{FN}	1.51e-1
u_{FP}	6.98e-2	u_{FN}	8.06e-3	g_{K1}	1.00	g_{K2}	9.21e-1
g_{K3}	8.03e-1	g_{K4}	1.88e-1	g_{Klim}	2.51e-1	g_{D1}	6.81e-1
g_{D2}	4.95e-1	g_{D3}	2.17e-1	g_{D4}	3.13e-1	g_{Dlim}	2.47e-1
g_{F1}	8.02e-1	g_{F2}	2.14e-1	g_{F3}	1.30e-1	g_{F4}	4.64e-1
g_{Flim}	2.57e-1						
ElasticPP Material Parameters							
E_{pp}	8 kN/mm	ϵ_{py}	1.00e-3				

Notes: In the table, F_{P1} , F_{P2} , F_{P3} , F_{P4} are the positive forces. F_{N1} , F_{N2} , F_{N3} , F_{N4} are the negative forces. Δ_{P1} , Δ_{P2} , Δ_{P3} , Δ_{P4} are the positive displacements. Δ_{N1} , Δ_{N2} , Δ_{N3} , Δ_{N4} are the negative displacements. r_{DP} , r_{DN} , r_{FP} , r_{FN} , u_{FP} , u_{FN} are the parameters that control the recovery path of hysteresis curves. g_{K1} , g_{K2} , g_{K3} , g_{K4} , g_{Klim} , g_{D1} , g_{D2} , g_{D3} , g_{D4} , g_{Dlim} , g_{F1} , g_{F2} , g_{F3} , g_{F4} , g_{Flim} are the parameters that control the degradation of the hysteretic curves. E_{pp} is the initial stiffness of ElasticPP Material. ϵ_{py} is the yield displacement of ElasticPP Material.

CONCLUSIONS

1. It was found that the initial stiffness, yield load, and maximum load of *Blockhaus* specimens can be improved by increasing the number and diameter of wooden dowels. However, the number of dowels had the most noticeable impact on the shear properties. Compared with the single-dowel specimens, the initial stiffness and peak load of the double-dowel specimens were increased by 100.4% and 108.0%, respectively, and those of the three-dowel specimens were increased by 278.0% and 196.2%, respectively.

2. The application of the initial pretension load significantly increased the initial stiffness and ultimate load of the specimen and improved the energy dissipation capacity of the specimen. For single dowel and double dowel specimens, the initial stiffness of specimens with initial pretension load increased 165.2% and 89.8%, respectively.
3. Due to the randomness of timber properties, there was a large difference between specimens in the peak load and load-decreasing stage. In this paper, a simplified numerical model was established in Opensees. The parameters were identified in Matlab and Opensees using modified Genetic Algorithm, and the parameters were obtained by considering all test data of specimens and adding them to the objective function.
4. The identified parameters were applied to the single-dowel and multi-dowel specimens. Through comparing the hysteresis curves of the test and the numerical model, it can be seen that the numerical model results were in good agreement with the test results. Therefore, the validity of the finite element model and the identified parameters was verified.

ACKNOWLEDGMENTS

The authors are grateful for the support of National Natural Science Foundation of China, Grant. No. 51878344.

REFERENCES CITED

- Bedon, C., and Fragiaco, M. (2019). "Experimental and numerical analysis of in-plane compressed unprotected log-haus timber walls in fire conditions," *Fire Safety Journal* 107, 89-103. DOI: 10.1016/j.firesaf.2017.12.007
- Branco, J. M., and Araújo, J. P. (2010). "Lateral resistance of log timber walls subjected to horizontal loads," in: *Proceedings of the 11th World Conference on Timber Engineering*, Trentino, Italy, pp. 2876-2885.
- Branco, J. M., and Araújo, J. P. (2012). "Structural behaviour of log timber walls under lateral in-plane loads," *Engineering Structures* 40, 371-382. DOI: 10.1016/j.engstruct.2012.03.004
- Branco, J. M., Lourenço, P. B., and Aranha, C. A. (2013). "Seismic analysis of a 2-storey log house," *Advanced Materials Research* 778, 478-485. DOI: 10.4028/www.scientific.net/AMR.778.478
- EN 408:2010+A1 (2012). "Timber structures – Structural timber and glued laminated timber – Determination of some physical and mechanical properties," European Committee for Standardization, Brussels, Belgium.
- EN 1995-1-1 (2004). "Eurocode 5 – Design of timber structures – Part 1-1: General-common rules and rules for buildings," European Committee for Standardization, Brussels, Belgium.
- EN 1998-1 (2004). "Eurocode 8 – Design of structures for earthquake resistance – Part 1: General rules, seismic actions and rules for buildings," European Committee for Standardization, Brussels, Belgium.

- EN 12512 (2001). “Timber structures – Test methods – Cyclic testing of joints made with mechanical fasteners,” European Committee for Standardization, Brussels, Belgium.
- Giovannini, T., Grossi, P., Sartori, T., and Tomasi, R. (2014). “Blockhaus system: Experimental characterization of corner joints and shear walls,” in: *Proceedings of the 13th World Conference on Timber Engineering*, Quebec City, Canada, pp. 10-14.
- Graham, D. A., Carradine, D. M., Bender, D. A., and Dolan, J. D. (2010). “Performance of log shear walls subjected to monotonic and reverse-cyclic loading,” *Journal of Structural Engineering* 136(1), 37-45. DOI: 10.1061/(ASCE)ST.1943-541X.0000035
- Grossi, P., Sartori, T., Giongo, I., and Tomasi, R. (2016). “Analysis of timber log-house construction system via experimental testing and analytical modelling,” *Construction and Building Materials* 102, 1127-1144. DOI: 10.1016/j.conbuildmat.2015.10.067
- Hirai, T., Kimura, T., Yanaga, K., Sasaki, Y., and Koizumi, A. (2004). “Lateral resistance of log constructions,” in: *Proceedings of the 8th World Conference on Timber Engineering*, Lahti, Finland, pp. 251-254.
- JGJ/T 101 (2015). “Specification for seismic test of buildings,” Architecture and Building Press, Beijing, China.
- Lam, F., Schulte-Wrede, M., Yao, C. C., and Gu, J. J. (2008). “Moment resistance of bolted timber connections with perpendicular to grain reinforcements,” in: *Proceedings of the 10th World Conference on Timber Engineering*, Miyazaki, Japan, pp. 978-985.
- Li, Z., He, M., and Wang, K. (2018). “Hysteretic performance of self-centering glulam beam-to-column connections,” *Journal of Structural Engineering* 144(5), article ID 04018031. DOI: 10.1061/(ASCE)ST.1943-541X.0002012
- Sciomenta, M., Bedon, C., Fragiaco, M., and Luongo, A. (2018). “Shear performance assessment of timber log-house walls under in-plane lateral loads via numerical and analytical modelling,” *Buildings* 8(8), article 99. DOI: 10.3390/buildings8080099
- Sciomenta, M., Rinaldi, V., Bedon, C., and Fragiaco, M. (2020). “Application of modal-displacement based design method to multi-story timber Blockhaus structures,” *Applied Sciences* 10(11), article 3889. DOI: 10.3390/app10113889
- Scott, R. J., Leichti, R. J., and Miller, T. H. (2005a). “An experimental investigation of foundation anchorage details and base shear capacity for log buildings,” *Forest Products Journal* 55(4), 38-45.
- Scott, R. J., Leichti, R. J., and Miller, T. H. (2005b). “Finite-element modeling of log wall lateral force resistance,” *Forest Products Journal* 55(9), 48-54.
- Tomasi, R., and Piazza, M. (2013). “Investigation of seismic performance of multi-storey timber buildings within the framework of the SERIES Project,” in: *Proceedings of the 2nd International Conference on Structure and Architecture*, Guimaraes, Portugal, pp. 82-89.
- Wang, M., Gu, X., Song, X., and Wu, Y. (2016). “Experimental study on bolted glued laminated timber connections with slotted-in steel plates under pure bending and combined shear and bending,” *Journal of Building Structures* 37(4), 64-72.
- Wang, M., Song, X., and Gu, X. (2018). “Three-dimensional combined elastic-plastic and damage model for nonlinear analysis of wood,” *Journal of Structural Engineering* 144(8), article ID 04018103. DOI: 10.1061/(ASCE)ST.1943-541X.000209
- Wang, M., Song, X., Gu, X., and Yin, X. (2019). “Variability analysis of bolted glulam beam-to-column connections,” *China Civil Engineering Journal* 52(7), 13-22.

Wang, T. (2018). *Research on Seismic Behavior of Glulam Frame Log Cabin Wall Structure*, Master's Thesis, Nanjing Tech University, Nanjing, China.

Article submitted: November 16, 2023; Peer review completed: March 2, 2024; Revised version received and accepted: March 20, 2024; Published: April 22, 2024.

DOI: 10.15376/biores.19.2.3681-3698